Molecular Dynamics Simulations Combined with Large Angle X-ray Scattering Technique for the Determination of the Structure, Conformation, and Conformational Dynamics of Polyphosphazenes in Amorphous Phase: Study of Poly[di(4-methylphenoxy)phosphazene]

Ruggero Caminiti,[†] Mario Gleria,[‡] Kenny B. Lipkowitz,[§] Giuseppe M. Lombardo,[||] and Giuseppe C. Pappalardo*,[||]

Contribution from the Istituto Nazionale per la Fisica della Materia, Dipartimento di Chimica, Università La Sapienza, p.le A. Moro 5, 00185 Roma, Italy, Istituto FRAE, CNR, Via Romea 4, 35020 Legnaro, Padova, Italy, Department of Chemistry, Indiana University−Purdue University at Indianapolis, Indianapolis, Indiana 46202, and Dipartimento di Scienze Chimiche, Cattedra di Chimica Generale, Facoltà di Farmacia, Università di Catania, Viale A. Doria 6, 95125 Catania, Italy

Received May 31, 1996. Revised Manuscript Received October 7, 1996[⊗]

Abstract: Suitable parameter sets for the CHARMm force field were derived using the Dinur−Hagler energy second-derivative procedure, on the basis of SCF calculations at the 6-31G* level, for the uncommon structural units in poly(phenoxyphosphazenes) [P═N, P−N, P−X (X = aryloxy)]. It is shown that application of molecular dynamics (MD) simulations, in combination with experimental energy dispersive X-ray diffraction (EDXD) measurements, provide unambiguous structural and conformational information on amorphous polymers. The procedure for the analysis of the EDXD data involves comparison of computed atom−atom radial distribution function (RDF) curve from MD simulations for the various polymer backbone conformations, with the RDF obtained from experimental X-ray scattering data. The applicability of this combined experimental/computational methodology is illustrated on the amorphous poly[di(4-methylphenoxy)phosphazene] (PMPP). The results showed that (i) the backbone conformation is safely $[TC]_n$ rather than $[T_3C]_n$ and (ii) the computed RDFs are best assessed by using a MD simulation technique that avoids assumption of static chain conformation and the needed best fit of the distance dependent parameters s_{jk}. In this method of analysis, the RDF that to be compared with the experimental one is directly calculated from all microstates collected during the entire simulation period. Validation of the polymer model provides a complete picture, otherwise experimentally inaccessible, of the internal fluctuations of the polymeric chains. The computational protocol delineated for analysis of EDXD data is general and its application specifically necessary when highly flexible amorphous polymers are involved.

Introduction

Molecular dynamics (MD) simulations[1,2] represent a major focus of modern theory directed toward understanding the structural features, energetics, and dynamics of macromolecules.

One macromolecular system of significance is the class of polymers known as polyphosphazenes. These are technologically important materials having properties as thermal stability,[3] flame resistance,[4] and chemical inertness.[5] Polyphosphazenes bearing different types of phenoxide substituents are interesting substrates due to their flame retardant characteristics,[6] high oxygen index values,[7] and low smoke evolution properties.[8] Furthermore, these materials are suitable for implantation purposes,[9,10] for synthesis of hydrolytically unstable polyphosphazenes applicable as drug-delivering systems,[11−13] of water-insoluble materials bearing biologically active surface groups (e.g., heparin),[14,15] and of water-swellable polymeric gels.[16] The potential applications of polyphosphazenes in the biomedical field[17] and their use as electric materials,[18−24] nonlinear optics

* Author to whom correspondence should be addressed.
[†] Università La Sapienza.
[‡] Istituto FRAE, CNR.
[§] Indiana University−Purdue University at Indianapolis.
[||] Università di Catania.

[⊗] Abstract published in *Advance ACS Abstracts,* January 1, 1997.

(1) Allen, M. P.; Tildesley, D. J. In *Computer Simulations of Liquids*; Clarendon Press: Oxford, 1987.
(2) *Computer Simulation of Biomolecular Systems: Theoretical and Experimental Applications*; Van Gunsteren, W. F., Weiner, P. K., Wilkinson, A. J., Eds.; ESCOM Science Publishers B. V.: Leiden, The Netherlands, 1993; Vol. 2.
(3) Kyker, G. S.; Antkowiak, T. A. *Rubber Chem. Technol.* **1974**, *47*, 32.
(4) Tate, D. P. *J. Polym. Sci. Polym. Symp.* **1974**, *48*, 33.
(5) Allcock, H. R. In *Phosphorus-Nitrogen Compounds*; Academic Press: New York, 1972.
(6) DiEdwardo, A. H.; Zitomer, F.; Stuetz, D.; Singler, R. E.; Macaione, D. *Org. Coat. Prep.* **1976**, *36*, 737.
(7) Thompson, J. E.; Reynard, K. A. *J. Appl. Polym. Sci.* **1977**, *21*, 2575.
(8) Quinn, E. J.; Althouse, B. M.; Potin, P. In *Proceedings of the Symposia Chem. Comb. Toxic MARM*; Millerville, PA, May 1988.
(9) Wade, C. W. R.; Gourlay, S.; Rice, R.; Hegyeli, A.; Singler, R. E.; White, J. In *Organometallic Polymers*; Carraher, C. E., Sheats, J. E., Pittman, C. U., Eds.; Academic Press: New York, 1978; pp 289.
(10) Goedemoed, J. H.; DeGroot, K. *Makromol. Chem. Macromol. Symp.* **1988**, *19*, 341.
(11) Grolleman, C. W. J.; DeVisser, A. C.; Wolke, J. G. C.; Van der Goot, H.; Timmerman, H. *J. Controlled Release* **1986**, *3*, 143.
(12) Grolleman, C. W. J.; DeVisser, A. C.; Wolke, J. G. C.; Van der Goot, H.; Timmerman, H. *J. Controlled Release* **1986**, *4*, 133.
(13) Grolleman, C. W. J.; DeVisser, A. C.; Wolke, J. G. C.; Van der Goot, H.; Timmerman, H. *J. Controlled Release* **1986**, *4*, 119.
(14) Neenan, T. X.; Allcock, H. R. *Biomaterials* **1982**, *3*, 78.
(15) Lora, S.; Carenza, M.; Palma, G.; Pezzin, G.; Caliceti, P.; Battaglia, P.; Lora, A. *Biomaterials* **1991**, *12*, 275.
(16) Allcock, H. R.; Kwon, S.; Riding, G. H.; Fitzpatrick R. J.; Bennett, J. L. *Biomaterials* **1988**, *9*, 509.

S0002-7863(96)01858-6 CCC: $14.00

polymers,[25,26] liquid crystals,[27−30] and membranes[31−33] have been extensively exploited.

It is clear that understanding the properties of this important class of materials at the atomic level would enhance our ability to create second-generation materials with enhanced or new properties. Application of MD for simulating these materials would provide the following: (i) an ability to monitor the internal molecular fluctuations, thus revealing functional properties especially for a homologous or congeneric series; (ii) the ability to generate microscopic level information that can be correlated directly with experimentally detectable macroscopic properties through judicious use of statistical thermodynamics theories; (iii) the capability to fully explore most of conformational space, especially by implementing high-temperature MD runs; (iv) the capacity to help refine molecular structures using experimental data, especially X-ray diffraction data for crystalline and amorphous solid phases and NMR data such as NOE intensities, relaxation times, and coupling constants in the liquid phase.

The ability of predicting macroscopic properties of polyphosphazenes based on microscopic structures derived from MD simulations has fundamental impact on the design of new materials with predetermined technological requisites. To accomplish this one must ensure that not only are the molecular simulations carried out on a long enough time scale to sample a significant volume of phase space but that one also selects a suitable unit or fragment of the material to serve as the model of the real system (as well as its environment). Moreover, a suitable statistical mechanical ensemble must be implemented to allow direct comparisons with certain experimental results.

More fundamental, however, is a proper choice of potential energy functions for the simulation. This is critical because the potential energy functions ultimately define the shape of the molecule's potential energy surface. The potential energy surface consequently dictates where the energy minima exist (giving rise to structural information), and the steepness or shallowness of the surface in turn defines the dynamical properties of the polymer. For polyphosphazenes, the force fields must be able to distinguish between double and single bonds, account for electron delocalization, and satisfactorily determine bond and torsion angles that agree with experiment. Most valence force fields commonly used today such as CHARMm,[34] MM2 and MM3,[35] and others can do this. Hence, both the form of the potential functions and their associated parameter set must be well-selected to ensure meaningful results.

MD simulations have not been applied until now to phosphazenic compounds, primarily due to the lack of suitable parameter sets for bonds and atoms of the uncommon structural units in these polymers [P═N, P−N, P−X (X = halogen, alkyl, alkyloxy, aryloxy, etc.)]. In the present work, we therefore first overcome this problem by deriving phosphazene parameters for use in the CHARMm force field. To accomplish this we rely on the technique of energy derivatives obtained from ab initio quantum mechanics as outlined by Dinur and Hagler.[36]

Obtaining structures of high accuracy and precision is clearly of great importance if maximal insight is to be obtained into the relationships between the three-dimensional structure and properties of the material, including the identification of subtle structural differences between similar polymers, or the conformational changes that accompany modifications of mechanical characteristics of a polymer. However, little is known about the molecular structures of polyphosphazenes in the solid phase due to multiple limitations of the X-ray diffraction techniques when applied to these polymers (low resolution of the diffraction patterns, low degree of crystallization of the samples, and thus high R factor values, etc.). For this reason, the most recent and accurate crystal structures of polyphosphazenes are concerned only with samples of highly oriented fibers of poly(dichlorophosphazene),[37] poly(dimethylphosphazene),[38] and poly[di(3,4-methylphenoxy)phosphazene][39] (PDMP).

Large-angle X-ray scattering (LAXS) is a powerful technique for determining structural parameters (interatomic distances) of amorphous systems.[40,41] In particular, energy dispersive X-ray diffraction (EDXD) has been recognized to be a suitable tool in the investigation of such systems because of its speed and reliability compared to those of a traditional angular scanning diffractometer.[42−44]

Our goals are to develop experimental and computational tools capable of providing the structural, energetic, and dynamic features of semicrystalline and amorphous materials. In this paper, we focus on phosphazenic polymers because of their global importance in both science and technology. However, what is described herein is applicable to any and more amorphous polymeric materials. The major impediment to understanding the structural features of these and related polymeric systems is that they have low crystallinity or, more

(17) Allcock, H. R. In *Biodegradable Polymers as Drug Delivery Systems*; Chasin, M., Langer R., Eds.; Marcel Dekker: New York, 1990; p 163.
(18) Allcock, H. R.; Dodge, J. A.; Van Dyke, L. S.; Martin, C. R. *Chem. Mater*. **1992**, *4*, 780.
(19) Kimura, T.; Kajiwara, M. *J. Inorg. Organomet. Polym*. **1992**, *2*, 431.
(20) Inoue, K.; Nishikawa, Y.; Tanigaki, T. *Macromolecules* **1991,** *24*, 3464.
(21) Inoue, K.; Nishikawa, Y.; Tanigaki, T. *J. Am. Chem. Soc*. **1991**, *113*, 7609.
(22) Ganapathiappan, S.; Chen, L. K.; Shriver, D. F. *J. Am. Chem Soc.* **1989**, *111*, 4091.
(23) Saraceno, R. A.; Riding, G. H.; Allcock, H. R.; Ewing, E. G. *J. Am. Chem. Soc*. **1988**, *110*, 980.
(24) Saraceno, R. A.; Riding, G. H.; Allcock, H. R.; Ewing, E. G. *J. Am. Chem. Soc*. **1988**, *110*, 7254.
(25) Allcock, H. R.; Dembek, A. A.; Kim, C.; Devine, R. L. S.; Shi, Y.; Steier, W. H.; Spangler, C. W. *Macromolecules* **1991**, *24*, 1000.
(26) Dembek, A. A.; Kim, C.; Allcock, H. R.; Devine, R. L. S.; Steier, W. H.; Spangler, C. W. *Chem. Mater*. **1990**, *2*, 97.
(27) Moriya, K.; Miyata, S.; Yano, S.; Kajiwara, M. *J. Inorg. Organomet. Polym.* **1992**, *2*, 443.
(28) Singler, R.; Willingham, R. A.; Noel, C.; Friedrich, C.; Bosio, L.; Atkins, E. D. T. *Macromolecules* **1991**, *24*, 510.
(29) Allcock, H. R.; Kim, C. *Macromolecules* **1990**, *23*, 3881.
(30) Kim, C.; Allcock, H. R. *Macromolecules* **1987**, *20*, 1726.
(31) Allcock, H. R.; Nelson, C. J.; Coggio, W. D.; Manners, I.; Koros, W. J.; Walker, D. R. B.; Pessan, L. A. *Macromolecules* **1993**, *26*, 1493.
(32) Gaeta, S. N.; Zhang, H. C.; Drioli, E.; Basile, A. *Desalination* **1991**, *80*, 181.
(33) Drioli, E.; Zhang, S. M.; Basile, A.; Golemme, G.; Gaeta, S. N.; Zhang, H. C. *Gas Sep. Purif.* **1991**, *5*, 252.
(34) Brooks, B. R.; Bruccoleri, R. E.; Olafson, B. D.; States, D. J.; Swaminathan, S.; Karplus, M. *J. Comput. Chem*. **1983**, *4*, 187.
(35) Burkert, U.; Allinger, N. L. In *Molecular Mechanics*; ACS Monograph 177; American Chemical Society: Washington, DC, 1982.
(36) Dinur, U.; Hagler, A. T. In *Reviews in Computational Chemistry*; Lipkowitz, K. B., Boyd, D. B., Eds.; VCH Publishers: New York, 1991; Vol. 2, pp 99−164.
(37) Chatani, Y.; Yatsuyanagi, K. *Macromolecules* **1987**, *20*, 1042.
(38) Meille, S. V.; Poletti, A. R.; Gallazzi, M. C.; Gleria, M.; Bruckner, S. *Polymer* **1992**, *33*, 2364.
(39) Burkhart, C. W.; Gillette, P. C.; Lando, J. B. *J. Polym. Sci., Polym. Phys. Ed*. **1983**, *21*, 2349.
(40) Caminiti, R.; Munoz Roca, C.; Beltran Porter, D.; Rossi, A. *Z. Naturforsch.* **1988**, *43a*, 591.
(41) Atzei, D.; Caminiti, R.; Sadun, C.; Bucci, R.; Corrias, A. *Phosphorus, Sulfur Silicon Relat. Elem.* **1993**, *79*, 13.
(42) Egami, T.; Gunterodt, H. J.; Beck, H. *Glassy Metals*; Springer-Verlag: Berlin, 1981; Vol. 1, p 25.
(43) Capobianchi, A.; Paoletti, A. M.; Pennesi, G.; Rossi, G.; Caminiti, R.; Ercolani, C. *Inorg. Chem.* **1993**, *3*, 4635.
(44) Atzei, D.; De Filippo, D.; Rossi, A.; Caminiti, R.; Sadun, C. *Spectrochim. Acta* **1995**, *51*, 11.

commonly, they are amorphous materials, making traditional X-ray diffraction techniques difficult or impossible.

To overcome this limitation we apply EDXD to derive the radial distribution function (RDF) from X-ray scattering data. Then, for the first time, we apply MD simulations to assist in data analysis. More specifically, we use a quantum mechanically derived set of force field (FF) parameters for CHARMm and we describe two computational protocols for predicting RDFs derived from EDXD experiments. On the basis of this application of theory combined with experiment, we provide incontrovertible evidence that the polymeric chain backbone conformation of poly[di(4-methylphenoxy)phosphazene] (PMPP, Scheme 1) exists in the $[TC]_n$ (*i.e.*, (*trans, cis, trans, cis*)), rather than the $[T_3C]_n$, (*i.e.*, (*trans, trans, trans, cis*)) state.

It is noteworthy that, after verification of consistency between the MD simulation model and the EDXD data, the MD model is also able to detect details, otherwise inaccessible, on the internal fluctuations of geometries and conformations along the polymer chains.

Scheme 1

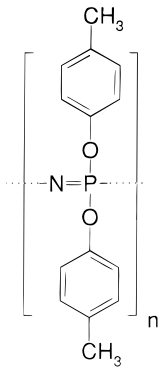

Derivation of Force Field Parameters

The CHARMm[34] force field parameters have been developed for linear polyphosphazenes using the Dinur and Hagler[36] method of energy derivatives from ab initio data. The basic assumption has been made that the ab initio and the FF-calculated potential energy surfaces have the same shape, and thus $E^{QM} = E^{FF} + K$ with $K =$ constant. Accordingly, the derivatives at a given point will have the same value in both ab initio and FF cases.

The use of energy derivatives allows deletion of the undesired energy terms so that we may obtain each calculated term completely pure from the other interactions. This makes the parameters transferable from molecule to molecule and thus suited for application to polyphosphazenic chains independently from the substituents they bear.

In fact, the total energy of the molecule in the FF calculation can be written as in eq 1:

$$E = E_S + E_b + E_{UB} + E_{tor} + E_{nb} = \sum V_S(b) + \sum V_b(\theta) + \sum V_{UB}(l) + \sum V_{tor}(\phi) + \sum V_{nb}(r) \quad (1)$$

In which the energy terms are represented by V_S (bond stretching), V_b (bending), V_{UB} (Urey−Bradley), V_{nb} (nonbonded), and V_{tor} (torsional). The energy first derivative with respect to the *i*th atom position then results

$$\frac{\partial E^{QM}}{\partial r_i} = \frac{\partial E^{FF}}{\partial r_i} = \frac{\partial V_S(b_i)}{\partial r_i} + \frac{\partial}{\partial r_i}\sum_{kj} V_b(\theta_{ijk}) + \frac{\partial}{\partial r_i}\sum_{k} V_{UB}(l_{ik}) + \frac{\partial}{\partial b_i}\sum_{m} V_{nb}(r_{im}) + \frac{\partial}{\partial r_i}\sum_{jkl} V_{tor}(\phi_{ijkl}) \quad (2)$$

while the second derivative with respect to the position of atoms *i* and *j* is (with atom *i* bonded to atom *j*)

$$\frac{\partial^2 E^{QM}}{\partial r_i \partial r_j} = \frac{\partial^2 E^{FF}}{\partial r_i \partial r_j} = \frac{\partial^2 V_S(b_i)}{\partial r_i \partial r_j} + \frac{\partial^2}{\partial r_i \partial r_j}\sum_{k} V_b(\theta_{ijk}) + \frac{\partial^2}{\partial r_i \partial r_j}\sum_{k,l} V_{tor}(\theta_{ijkl}) \quad (3)$$

Equations 2 and 3 show that increasing the order of the energy derivative will decrease the number of terms contributing to its value.

Equation 3 represents the off-diagonal elements of the Cartesian Hessian matrix for atoms *i* and *j*, and is related to the interactions between these two atoms purified from the other energy terms. The analytical method we followed for calculating the energy second derivatives with respect to a given parameter (bond length, bend angle, torsional angle, 1−3 distance for UB term) from these matrix elements is described in a previous paper[45] in which the FF parameters were calculated for cyclic phosphazenes for use in MM2 and CHARMm programs.

The determination of the CHARMm force field parameters was performed using quantum mechanical ab initio calculations (GAUSSIAN92[46]) at the 6-31G* level on model compounds that contained short P−N chains able to meet the Hopfinger−Pearlstein guidelines.[47]

The procedures for obtaining the CHARMm parameters using the energy second derivatives requires the calculation of the minimum energy structure of the molecules chosen as model compounds. Since the values of the ab initio calculated energy second derivative depend on the specific valence coordinate, the assumption was made that the best value for the force constants K_A was that at the calculated ab initio equilibrium geometry of the model molecules.

The equilibrium values of each bond and angle were assumed to be the mean value for the specific type of bond length and bond angle in the ab initio calculated minimum energy structures. The l_0 and α_0 parameters were obtained by refinement of these values to best reproduce the ab initio structures.

In the derivation of the torsional parameters, the energy second derivative with respect to the torsion angle was obtained by means of the procedure described in detail by Dinur and Hagler.[48] For each torsional four-atom unit to be parametrized, an adequate model compound was selected following the Hopfinger−Pearlstein[47] directions.

Due to lack of accurate geometry data derived from X-ray diffraction analysis, accuracy of the calculated FF parameter set (shown in Table 1) was checked by the agreement found between FF and quantum mechanical geometries of the model compounds. Additionally the reliability of the procedure was

(45) Amato, M. E.; Lipkowitz, K. B.; Lombardo, G. M.; Pappalardo, G. C. *J. Mol. Struct.* **1995**, *372*, 69.
(46) Frish, M. J.; Trucks, G. W.; Head-Gordon, M.; Gill, P. M. W.; Wong, N. W.; Foresman, J. B.; Johnson, B. G.; Schlegel, H. B.; Robb, M. A.; Replogle, E. S.; Gomperts, R.; Andres, J. L.; Raghavachari, K.; Binkley, J. S.; Gonzales, C.; Martin, R. L.; Fox, D. J.; DeFrees, D. J.; Baker, J.; Stewart, J. J. P.; Pople, J. A. *GAUSSIAN 92, Revision D.2*; Gaussian Inc.: Pittsburgh, PA, 1993.
(47) Hopfinger, A. J.; Pearlstein, R. A. *J. Comput. Chem.* **1984**, *5*, 486.
(48) Dinur, U.; Hagler, A. T. *J. Comput. Chem.* **1990**, *11*, 1234.

Table 1. CHARMm Parameter Set for Polyphosphazenes

parameter	l_0 (Å)	k_s (kcal/ mol Å^2)	θ_0 (deg)	k_b (kcal/ (mol deg^2))	l_0 (Å)	k_{UB} (kcal/ (mol Å^2))
bond						
P—N	1.617	360.0				
P═N	1.550	568.0				
P—O	1.618	320.0				
bend						
P—N═P			145.0	28.0	3.022	115.0
N—P═N			117.0	54.0	2.701	50.0
N—P—O			108.7	22.7	2.629	58.2
N═P—O			124.3	82.3	2.801	25.9
O—P—O			102.0	51.8	2.515	45.9
P—O—C			125.6	12.4	2.660	102.2

parameter	$V(1)$ (kcal mol^{-1})	$V(2)$ (kcal mol^{-1})	$V(3)$ (kcal mol^{-1})	ϕ_0
torsional				
N—P═N—P	2.702	−1.707	0.020	0.0
N═P—N═P	−6.340	−1.028	−0.174	0.0
O—P═N—P	4.326	0.024	0.069	0.0
O—P—N═P	1.696	0.156	0.023	0.0
C—O—P—N	2.970	−0.583	0.195	0.0
C—O—P═N	2.667	−1.233	0.054	0.0
C—O—P—O	1.957	−0.900	0.079	0.0

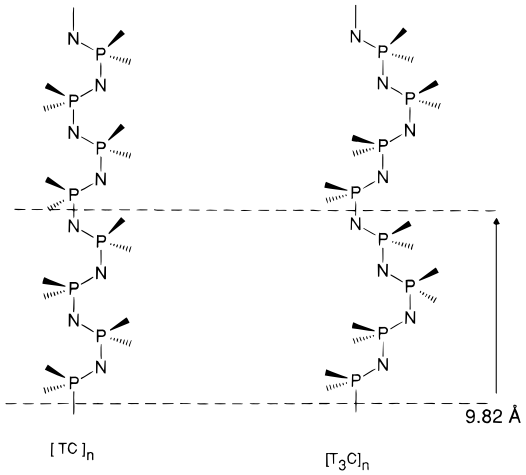

Figure 1. Possible planar backbone models $[TC]_n$ and $[T_3C]_n$ for the polymer chain of PMPP.

confirmed by the previous work,[45] in which theoretical data were compared to crystal structure data on a well-characterized cyclo(phenoxyphosphazene).

Molecular Dynamics Simulations

Protocols. MD calculations were performed with the CHARMm program using the FF parameters derived for poly(phenoxyphosphazenes). The IMAGE facility of the CHARMm program was used for reproducing the periodic boundary conditions (PBC) needed for the simulation of infinite polymers and/or crystalline state. The amorphous PMPP was assumed in a partially ordered state, since the used simulation temperature (298 K) is largely below the mesophase transition temperature (ca. 373−423 K) determined for PMPP.[49] Accordingly, the polymeric chains were oriented, by analogy, using the unit cell parameters determined[39] for PDMP in the crystal (orthorhombic unit cell with $a = 15.85$, $b = 19.43$, and $c = 9.85$ Å). The PMPP chain was arranged and studied in the two possible backbone conformational models (Figure 1) proposed for PDMP in the crystal,[39] (*i.e.*, $[T_3C]_n$ and $[TC]_n$).

The atomic charges required were set at the Mulliken values from ab initio 6-31G* level calculations for model compounds used in developing the FF parameters: P, 1.955; N, −1.113; O, −0.797; C(O), 0.376; C(H), −0.182; C(C), −0.364; H, 0.182. The SHAKE protocol as constraint for all CH bonds was used.

All of the simulations were run by starting from optimized structures with 2000 steps of steepest descent followed by a 20 ps equilibration at 298 K. Transients for 200 ps with a sampling interval of 0.1 ps were usually collected. The integration time step was 0.002 ps.

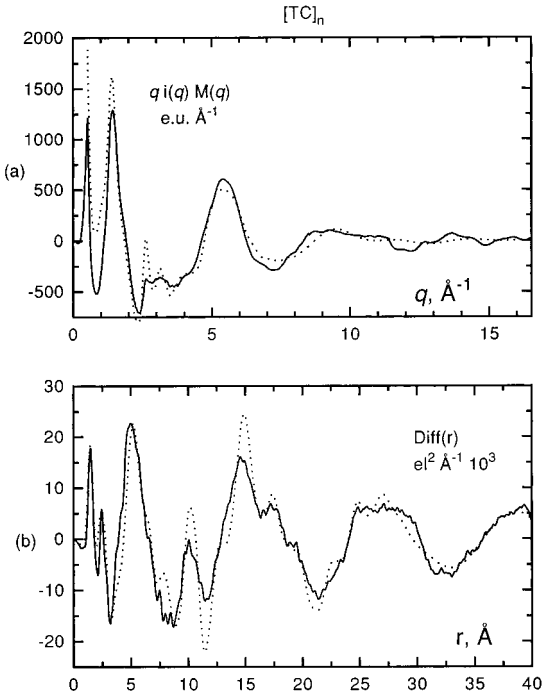

Figure 2. Comparison between experimentally (EDXD) observed (solid line) and calculated (dotted line) structure function (a) and related RDF (b) for $[TC]_n$ model of PMPP. Theoretical curves are calculated using the first method for data analysis.

Experimental Section

Sample. The PMPP sample was prepared starting from poly(dichlorophosphazene) $(NPCl_2)_n$. This was prepared by bulk thermal polymerization of hexachlorocyclophosphazene $(NPCl_2)_3$ under vacuum using sealed, heavy glass, ampules of about 200 mL volume. When the trimer/polymer mixture reached the right viscosity (visual checking of the lack of flowing for the melt system), the polymerization was stopped, the glass flask broken, and the obtained poly(dichlorophosphazene) was freed from the residual, unreacted trimer by vacuum sublimation. The freshly prepared poly(dichlorophosphazene) was successively dissolved in anhydrous dioxan, treated with an excess of 4-methylphenoxide ion (from NaH 60% and 4-methylphenol), refluxed for 3 days in the presence of tetrabutylammonium bromide, precipitated repeatedly in *n*-heptane, water, and methanol (in this order), and dried under vacuum, according to literature.[50] The obtained PMPP was characterized by IR and ^{31}P NMR spectroscopies. The differential scanning calorimetry (DSC) profile, performed using a Mettler DSC 30 calorimeter, showed a T_g transition at +6 °C, followed by an exothermal peak for the mesophase formation at 103 °C and by a second endothermal peak at 141 °C, attributed to the $T(1)$ value for the mesophase transition.

The average molecular weight M_w of PMPP, determined using gel permeation chromatography (GPC, water apparatus), was 2.5×10^6 with a molecular weight distribution of 10.6.

X-ray Experiments. The LAXS technique[40,41] allows much of the information on amorphous or quasi-amorphous materials to be extracted from the static structure function $i(q)$, where q indicates the scattering parameter (*i.e.*, $q = (4\pi/\lambda)(\sin\theta)$ or, equivalently, $q = (2/\hbar c)E(\sin\theta)$,

(49) Magil, J. H.; Riekel, C. *Makromol. Chem. Rapid Commun.* **1986**, *7*, 287.

(50) Singler, R. E.; Hagnauer, G. L.; Schneider, N. S.; Laliberte, B. R.; Sacher, R. E.; Matton, R. W. *J. Polym. Sci., Polym. Chem. Ed.* **1974**, *12*, 433.

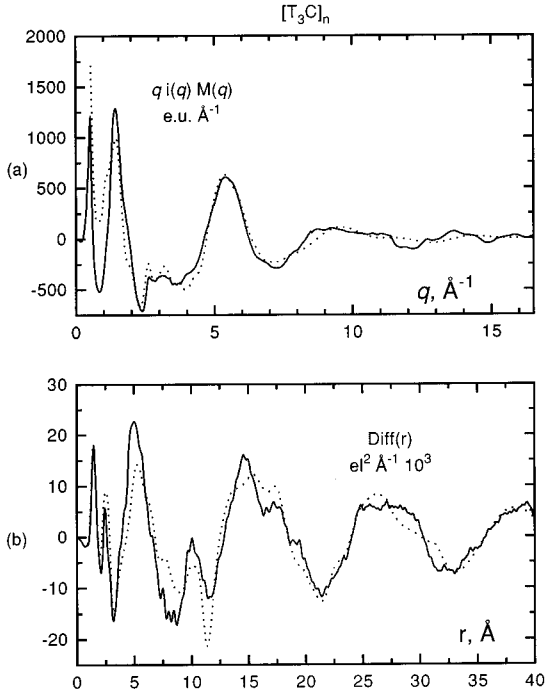

Figure 3. Comparison between experimentally (EDXD) observed (solid line) and calculated (dotted line) structure function (a) and related RDF (b) for $[T_3C]_n$ model of PMPP. Theoretical curves are calculated using the first method for data analysis.

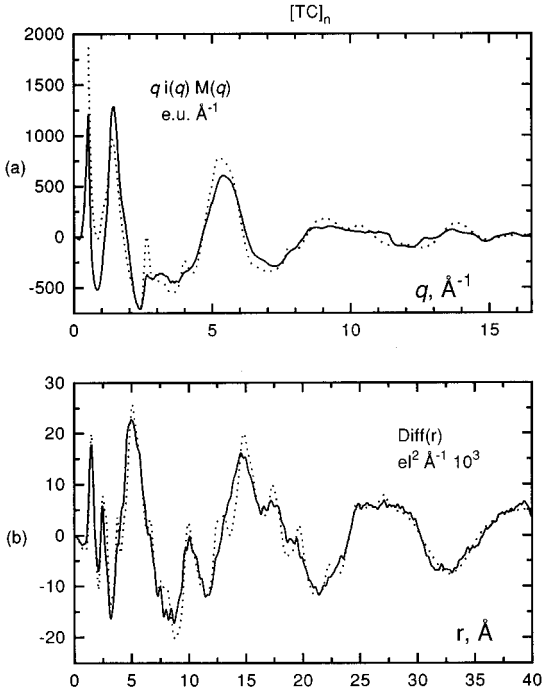

Figure 4. Comparison between experimentally (EDXD) observed (solid line) and calculated (dotted line) structure function (a) and related RDF (b) for $[TC]_n$ model of PMPP. Theoretical curves are calculated using the second method for data analysis.

where 2θ = scattering angle, λ = radiation wavelength, E = radiation energy, and c and $\hbar$ have their usual meaning.

Since q depends on both E and θ, to execute a scanning in the reciprocal q space (obtaining the diffraction pattern), it is possible either (fixed E) to perform an angular scanning or (fixed θ) to do an energetic scanning, by means of a polychromatic X-ray beam and an energy dispersive solid state detector (SSD) device.

In the present case, we used the second procedure, and diffraction data were collected with a noncommercial instrument,[51] comprised of a white X-ray beam source and a germanium SSD connected with a multichannel analyzer. Specified here are the working conditions used: (a) alimentation, high voltage = 45 kV, current = 35 mA, total power = 1575 W; (b) measurement angles (θ), 26.0, 15.5, 10.5, 8.0, 5.0, 3.5, 2.0, 1.0, 0.5°; (c) energy interval utilized 16−37 KeV (d) scattering parameter interval (q), 0.15−16.525 Å^{-1}.

After the necessary corrections of the experimental data collected,[52] such as escape peak suppression, normalization to incident radiation intensity, division by X-ray absorption and polarization coefficients, and elimination of inelastic scattering contributions, from the observed intensity $I(E,\theta)$, the static structure function $i(q)$ (shown in Figures 2a−5a as $qi(q)M(q)$; see below for $M(q)$) can be obtained. The Fourier transformation of the $S(q)$ function gives the radial distribution function (represented in Figures 2b−5b as $\mathrm{Diff}(r) = D(r) - 4\pi r^2\rho_0$)

$$D(r) = 4\pi r^2\rho_0 + 2r\pi^{-1}\int_0^{q_{max}} qi(q)\, M(q)\, \sin(rq)\, dq \qquad (4)$$

Here ρ_0 is the average electronic density of the sample

$$\rho_0 = (\sum_i n_i f_i(0))^2 V^{-1}$$

where V is the stoichiometric unit volume chosen, n_i = number of atoms "i" per unit volume, and f_i is the scattering factor per atom "i".[53] $M(q)$ is a modification function defined by

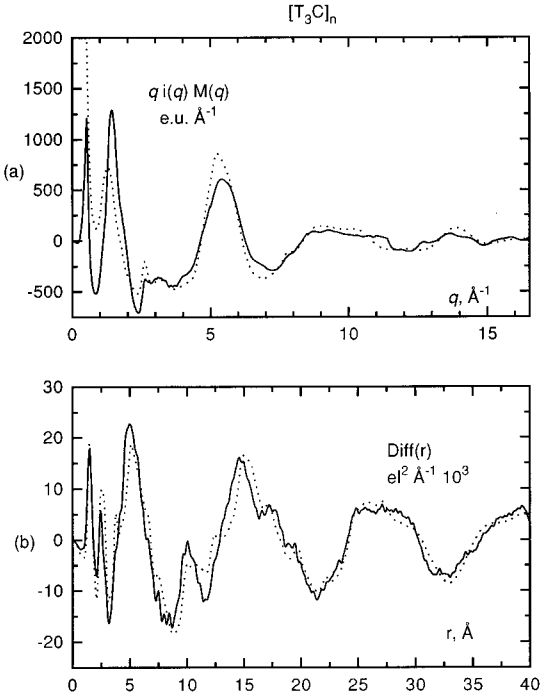

Figure 5. Comparison between experimentally (EDXD) observed (solid line) and calculated (dotted line) structure function (a) and related RDF (b) for $[T_3C]_n$ model of PMPP. Theoretical curves are calculated using the second method for data analysis.

$$M(\mathrm{q}) = \{f_P^2(0)/f_P^2(q)\}\, \exp(-0.01\, q^2) \qquad (5)$$

A more detailed description of the apparatus and technique is given elsewhere.[51,54,55]

(51) Caminiti, R.; Sadun, C.; Rossi, V.; Cilloco, F.; Felici, R. *XXV Italian Congress of Physical Chemistry*; Cagliari, Italy, 1991 *Idem*, It. Patent RM/93 01261484, 1993.

(52) Fritsch, G.; Keimel, D. A. *J. Mater. Sci. Eng.* **1991**, *A134*, 888.

(53) *International Tables for X-Ray Crystallography*; Kynoch Press: Birmingham, U.K.; 1974; Vol. 4.

(54) Nishikawa, K.; Iijima, T. *Bull. Chem. Soc. Jpn.* **1984**, *57*, 1750.

(55) Rossi Albertini, V.; Bencivenni, L.; Caminiti, R.; Cilloco, F.; Sadun, C. *J. Macromol. Sci., Phys.* **1996**, *35B* (2), 199.

(56) Bougeard, D.; Bremard, C.; De Jaeger, R.; Lemmouchi, Y. *Spectrochim. Acta, Part A* **1993**, *49*, 199.

Table 2. Final Values of the Adjusted Parameters (rms σ_{nm}) for the $[TC]_n$ Model

$0.0 < r \leq 1.6$ Å	$\sigma_1 = 0.075$
$1.6 < r \leq 3.0$	$\sigma_2 = 0.110$
$3.0 < r \leq 11.0$	$\sigma_3 = 0.300$
$r > 11.0$	$\sigma_4 = 0.400$

Data Analysis

The analysis of the RDF of X-ray data can be performed by comparison with a RDF curve produced by a theoretical model. The features of a RDF are determined by both the intersegmental chain conformations and the packing structure adopted by the neighboring polymer chains. To quantitatively assess the precise origins of the RDF contributions, two methods of analysis of the experimental scattering data were developed that may be applied to systems regardless of the degree of crystallinity. In both methods, only two chains (12 monomeric units per chain) were considered in the main cell. This allowed us to take into account a random disposal between the pairs of chains that determines the disappearance of well-resolved peaks in the long-range zone of the RDF curve.

In the first method, theoretical RDF peaks were calculated by a corresponding Fourier transform of the theoretical intensities for pairs of interactions (eq 6)

$$i(q) = \sum f_j f_k \frac{\sin(r_{jk}q)}{r_{jk}q} \exp(-{}^1/_2\sigma_{jk}^2 q^2) \qquad (6)$$

using the same sharpening factor (eqn 5) and the same scattering parameter interval (q) as for the experimental data and assuming the root mean square (rms) variations in the interatomic distance to be σ_{jk}.

For each $[T_3C]_n$ and $[TC]_n$ assumed structure model and related geometries, the σ_{jk} values were optimized by best fit of the theoretical intensities (calculated by eqn 6) to the experimental intensities. The same value of mean square deviation was assigned to interatomic distances r_{jk} falling within a preset range ($0 < r < 1.6$; $1.6 < r < 3$, etc.), so that the number of parameters was much smaller than the number of pair distances existing in the proposed model.

The average atomic coordinates we used were obtained from the last 2 ps of the simulations performed for $[T_3C]_n$ and $[TC]_n$ models of the polymeric chain.

The period of the X-ray ranges from 10^{-17} to 10^{-22} s. This interval is smaller than the integration time step (0.002 ps) of the simulation by at least 2 orders of magnitude. Therefore, while X photons interact with "frozen" atoms, the atomic $\langle x, y, z\rangle$ coordinates of the fluctuating chain during a long evolution time tend toward values which produce anomalously short interatomic distances. The choice of sampling the "last" 2 ps of each simulation was based on the reasonable assumption that these are more likely to represent the molecular equilibrium state.

The final values of rms σ_{jk} are reported in Table 2.

The second method aimed to avoid the above assumption of static chain conformation involving the best fit of σ_{jk} values as empirically adjusted parameters. This feature could be overcome by the MD simulations technique that is susceptible to directly provide the RDF for every possible combination of atomic-type pairs (P···P; P···N; P···C; etc.) (*i.e.*, $d_{nm}(r)$). Accordingly, the shape of the coherent scattering intensity curve was obtained through the RDF curves calculated from the snapshots collected along the entire evolution time of the simulation of each model. To this purpose, the discrete sum of eqn 6 must be transformed into an integral expression in terms of the continuous pair distribution functions $d_{nm}(r)$ (eq 7)

$$i(q) = \int_0^\infty 4\pi r^2 [f_P^2(q)c_P^2 d_{PP}(r) + f_P(q)f_N(q)c_P c_N d_{PN}(r) + ...] \times \frac{\sin(rq)}{rq}\,dr \qquad (7)$$

in which c_P and c_N are the atomic concentrations in the chosen model. This allows the calculation of the theoretical intensity curve from a MD simulation.

The possibility to verify the accuracy of predictions directly based on MD simulated models therefore constitutes a further meaningful aspect of this latter method of analysis of the EDXD data.

Results and Discussion

The observed structure function (SF) for the PMPP sample, in the form $qi(q)M(q)$, is reported (solid line) in Figures 2a−5a. The experimental RDF in the $\mathrm{Diff}(r) = D(r) - 4\pi r^2\rho_0$ form, obtained from the above SF, is presented (solid line) in Figures 2b−5b. The latter curve shows flattened peaks in the long-distance region thus featuring the amorphous state of PMPP. The two peaks at 1.50 and 2.4 Å were reasonably assigned to the P−N, P−O, O−C, and C−C bond distances and to the nonbonded interatomic distances O···N, O···O, O···C, and C···P, respectively, in a monomeric unit. The peaks at higher r values were attributed to intra- and/or interchain distances between atoms pertinent to separate monomeric units.

Results of the MD simulations were used to calculate theoretical RDFs using the first method above described in the Data Analysis section (method A). The attained SFs and RDFs (dotted line) for the assumed $[TC]_n$ and $[T_3C]_n$ backbone models of the chain are compared in Figures 2b and 3b, respectively, to the corresponding experimental curves.

In Figures 4 and 5, comparisons to the experimental data are made for SF and RDF curves calculated through the second method of data analysis (method B) that uses the complete evolution time of MD simulations for the proposed backbone models of crystalline PDMP.[39]

Inspection of Figures 2b and 3b shows some important features that allow us to discriminate between the two assumed models. In particular, in the range of 25−33 Å, the peak of the experimental RDF at ca. 27.5 Å is better reproduced by the curve of the $[TC]_n$ model than by that calculated for the $[T_3C]_n$. Moreover, the RDF calculated for $[T_3C]_n$ shows a shoulder in the range of 30−32.5 Å. In this range, where interchain interatomic distances predominate, the experimental curve presents a saddle which is well-reproduced by the $[TC]_n$ RDF. In the range of 12−22 Å, the $[T_3C]_n$ model shows an even greater marked difference than does the $[TC]_n$ model with respect to the experimental RDF. Indeed, within this region the $[T_3C]_n$ does not reproduce important peaks, but rather predicts a flattened and almost structureless zone. This is not the case of the alternative $[TC]_n$ model, whose shape and peaks of the RDF agree well with those of the experimental RDF in the range of 12−22 Å. When coming to the range of shorter interatomic distances, the two important peaks located at 2.4 and 5 Å are almost exactly reproduced by the $[TC]_n$ model, whereas this is not the case for the $[T_3C]_n$ model.

On the basis of the above illustrated comparisons between the shapes of the experimental RDF and of the RDFs calculated

(57) Grassi, A.; Lombardo, G. M.; Pappalardo, G. C. *J. Mol. Struct. (THEOCHEM)* **1994**, *311*, 101.
(58) Bandoli, G.; Gleria, M.; Lombardo, G. M.; Pappalardo, G. C. *J. Chem. Soc. Dalton Trans.* **1995**, 1749.

using the first procedure of data analysis (method A), it may be concluded that PMPP in the amorphous state adopts the $[TC]_n$ backbone model's shape and that the $[T_3C]_n$ alternate possibility is to be ruled out.

A further confirmation of this agreement comes from the root mean square deviation (rmsd) defined for both the SF and RDF where N is the number of points generating the curve.

$$\mathrm{rmsd}_{\mathrm{SF}} = \sqrt{\frac{\sum_j^N (i_j^{\mathrm{exptl}} - i_j^{\mathrm{calcd}})^2}{N}};$$

$$\mathrm{rmsd}_{\mathrm{RDF}} = \sqrt{\frac{\sum_j^N (\mathrm{RDF}_j^{\mathrm{exptl}} - \mathrm{RDF}_j^{\mathrm{calcd}})^2}{N}};$$

$$\Delta(\mathrm{rmsd}) = \left|\frac{\mathrm{rmsd(A)} - \mathrm{rmsd(B)}}{\mathrm{rmsd(A)}}\right| 100$$

Since we are comparing two different computational protocols for their possible application in analysis of amorphous materials, we use Δ(rmsd) where the rmsd for protocol A (the first method) is compared with protocol B (the second method). The choice in the favor of the $[TC]_n$ chain model of PMPP is also supported by the Δ(rmsd) for the complete SF and RDF [$\Delta(\mathrm{rmsd}_{\mathrm{SF}}) \cong \Delta(\mathrm{rmsd}_{\mathrm{RDF}}) \cong 10\%$ favoring the $[TC]_n$ model].

The results from the method B of data analysis, as shown by Figures 4 and 5, are quite consistent with the above conclusion obtained using the first method. In fact, a better agreement of the experimental RDF with the calculated RDF [Figure 4b] is very clearly detectable when one assumes the $[TC]_n$ model. The better quality of agreement in favor of the $[TC]_n$ chain model of PMPP is also evidenced by the Δ(rmsd) values [$\Delta(\mathrm{rmsd}_{\mathrm{SF}}) \cong \Delta(\mathrm{rmsd}_{\mathrm{RDF}}) \cong 27\%$].

Table 3. Averaged Energies (kcal mol^{-1}) per Monomeric Units of the $[TC]_n$ and $[T_3C]_n$ Models of PMPP as Calculated by MD[a]

energy	$[TC]_n$	$[T_3C]_n$
total	−827.15 (−778.24)	−731.39 (−754.56)
bond	7.77 (2.18)	5.29 (2.14)
angle	16.45 (10.15)	18.33 (11.69)
UB	11.78 (11.40)	16.08 (13.75)
dihedrals	14.96 (12.30)	21.66 (18.12)
impropers	1.52 (0.17)	1.57 (0.18)
electrostatic	−872.63 (−806.85)	−788.56 (−793.17)
VDW	−6.97 (−7.60)	−5.76 (−7.27)

[a] The corresponding energies of starting optimized models are also quoted in parentheses

Having established that the amorphous material, on average, assumes the $[TC]_n$ rather than the $[T_3C]_n$ shape, we next consider which of the two computational protocols of data analysis is better able to reproduce experiment. Above, we indicated that method B, which uses the full MD trajectory, appears better than method A. In terms of statistic agreement, we find the relative difference $\Delta(\mathrm{rmsd}_{\mathrm{RDF}})$ of the two methods of analysis on the calculated RDFs for the same $[TC]_n$ model to be in the favor of the second method by approximately 37%.

This confirms: (i) that the reliability of our proposed second method which in addition, with respect to the former, does not require the adjusting of parameters (σ_{jk}) by fitting and (ii) that the entire MD simulation (including the developed FF parameters) was representative of the studied molecular system and, accordingly, suited to give information on molecular features experimentally inaccessible.

The improved quality of the second method of analysis

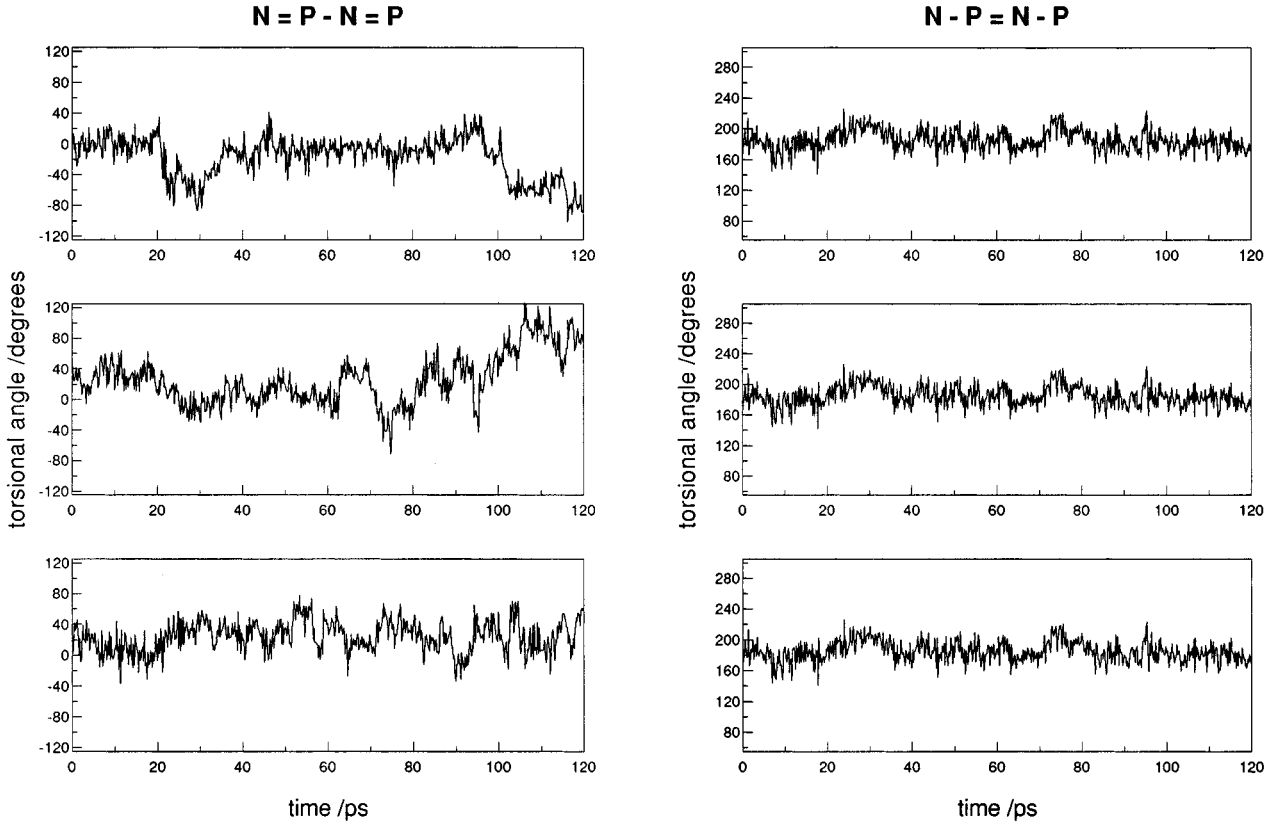

Figure 6. Time evolution traces for N═P−N═P and N−P═N−P torsional angles from MD simulations of PMPP in the $[TC]_n$ chain conformation. The three traces for each torsional angle refer to different fragments casually selected along the chain.

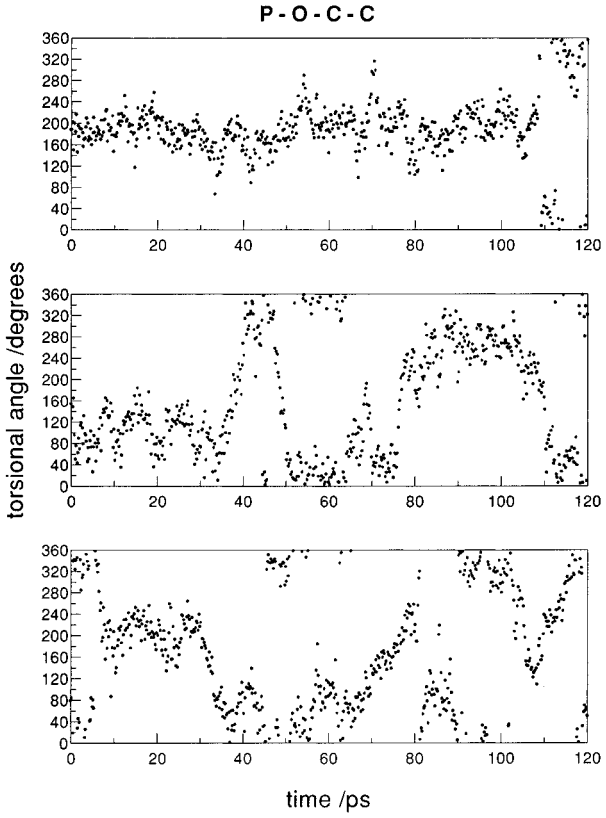

Figure 7. Time evolution traces for P—O—C—C torsional angle from MD simulations of PMPP in the $[TC]_n$ chain conformation. The traces refer to three POCC atomic sequences selected along the chain.

derives from the fact that this, by simulating the system dynamically instead of statically, is more adequate to reproduce the interatomic distance fluctuations typically featured in low-crystallinity materials having a high degree of internal conformational freedom.

The first method, based on a single fixed conformation of the molecules, describes the distance fluctuations by using a limited number of fitted parameters (σ_{jk}) assumed to be unchangeble within selected ranges of distances (Table 2) independently on the atom pairs. By focusing now on this particular aspect of the first method, the higher quality of our proposed second method of data analysis stems from its capability to monitor the distance fluctuations of the atomic pairs through use of trajectories of the whole MD simulation time. This is possible because the time scale of the MD simulation is faster than the frequency of the atomic vibrations and molecular conformational changes, so that MD is suited to provide the distribution probability of interatomic distances needed to reproduce at best the scattering intensity curve.

Interestingly, the average energies calculated by MD for monomeric units of both models (Table 3) also indicate that the $[TC]_n$ backbone arrangement is favored. The difference between the electrostatic terms (84.07 kcal mol^{-1}) mainly contributes to decreasing the total energy of the $[TC]_n$ model by 92.76 kcal mol^{-1} with respect to the $[T_3C]_n$ model. Table 3 quotes the calculated energy terms of the optimized models before starting simulations and shows that such differences in electrostatic terms as well as in total energies were smaller than those above. This is because these starting structures are just the first minimum encountered during the optimization and thus are scarcely representative of a true ensemble average. In contrast, the MD simulation scans all possible minima that are accessible during the evolution time thus providing statistically (Boltzmann-weighted) meaningful information.

Since detailed analysis of the trajectories can provide insights into the structure, conformational, and motion properties of the phosphazenic chain at the microscopic level, the MD results are presented in terms of time evolution of the torsional angles, N—P═N—P, N═P—N═P, and P—O—C—C in Figures 6 and 7.

While the chain backbone at the equilibrium fluctuates about the PN single bond by ca. ± 40−50°, the time evolution of the N—P═N—P torsional angles shows that they scarcely moved on the picosecond to nanosecond time scale. The P—O—C—C sets of torsional angles, as shown in Figure 7, fluctuate by accomplishing wide excursions up to 2π. Noteworthy are the concerted rotations of the pair of phenoxy rings attached to each P atom.

The average bond lengths and angles of PMPP are reported in Table 4. The alternate single—double P—N bond character is consistent with results from spectroscopic Raman P—N stretching studies[56] and ab initio (6-31G*) calculations for oligomeric chains of chlorophosphazenes.[57] The calculated extra-chain bond length values (P—O and O—C) agree with experimental data of cyclotriphosphazenes in the crystal.[58] The attained torsional angles about PN double and single bonds reproduce accurately the absolute values of the torsional angles reported by the most recent and highest precision X-ray diffraction studies on poly(dichlorophosphazene)[37] and poly(dimethylphosphazene)[38] in the glide conformation. The P—N and P═N bond distances and the bond angles also fall in the range of X-ray determined values for the above phosphazenic polymers.[37,38]

In Figure 8 is perspectively shown the quasi-planar conformation of PMPP at the thermal equilibrium, obtained by averaging the last 1000 steps of the MD simulation. A helix conformation of the chain in the amorphous state seems therefore to be ruled out.

In conclusion, the application of MD simulations, using quantum mechanically derived force field parameters, combined with EDXD data appears to be a general approach to solving otherwise intractable issues concerning structural features of materials that are amorphous in nature and not amenable to single-crystal X-ray diffraction. In this paper, we focused on a phosphazenic polymer, but the general methodology outlined here is extendable to any system and should be of use in many areas of the chemical sciences including materials science, polymer science, and biological chemistry. In this particular paper, the investigated phosphazenic material showing that (i)

Table 4. Averaged Values of Selected Bond Lengths (Å) and Angles (deg) of the $[TC]_n$ Model of PMPP as Calculated by MD Simulations[a]

bond lengths		bond angles		torsional angles	
P═N	1.51 (1.44[b], 1.56[c])	N—P═N	118.3 (115,[b] 112.5[c])	N—P═N—P	176.7 (175,[b] 174.1[c])
P—N	1.64 (1.67,[b] 1.59[c])	P═N—P	127.9 (131,[b] 135.9[c])	N═P—N═P	19.5 (31,[b] 23.9[c])
P—O	1.60 [1.58,[d] (mean)]	O—P═N	118.9	O—P═N═P	±62.8
O—C	1.40 [1.40[d] (mean)]	O—P—N	98.0	O—P—N═P	±88.1
		O—P—O	99.8 [96.6[d] (mean)]		
		C—O—P	123.2 [125.1[d] (mean)]		

[a] Recent experimental X-ray data for phosphazenic moieties are quoted in parentheses. [b] Reference 37. [c] Reference 38. [d] Reference 58.

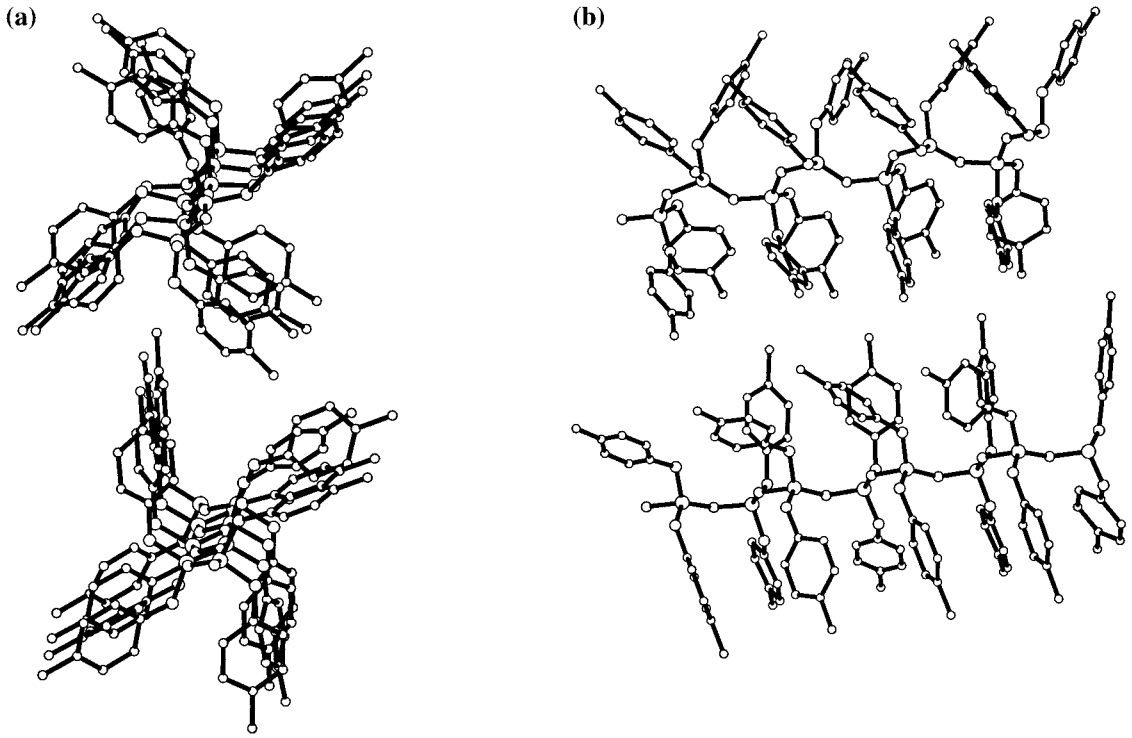

Figure 8. Two perspective views of a pair of chains of PMPP in the quasi-planar conformation from the averaged last 1000 steps of the MD simulation.

the assumed unit cell for PMPP, although containing a low degree of crystallinity, was correct and (ii) the backbone conformation of the amorphous PMPP polymer is $[TC]_n$.

In general, from the methodological point of view, the exploitation of the second method proposed here for producing models to analyze EDXD data is advisable when highly flexible molecules, such as amorphous polymers, are dealt with, providing MD simulations using a reliable FF method are accessible.

Acknowledgment. The contribution of one of us (K. B. Lipkowitz) to this paper was brought to fruition as a result of a visit in the spring 1996 to the Dipartimento di Chimica, Università di Catania, Italy, supported by CNR of Italy (grant code AI95.00018.03). This work was partially supported by MURST of Italy (Progetto Nazionale "Chimica dei Materiali").

JA961858K